ACS OMEGA

http://pubs.acs.org/journal/acsodf

Article

Zinc Metal–Organic Framework Growing on the Surface of Fruit Peels and Its Photocatalytic Activity

Lu Liu, Liqin Cao,* Hongyan Niu, and Jide Wang

Cite This: *ACS Omega* 2021, 6, 10187–10195

Read Online

ACCESS | Metrics & More | Article Recommendations | Supporting Information

ABSTRACT: The development of water treatment materials using environmentally friendly natural biomasses as substitutes plays an increasingly important role in environmental protection. Zeolitic imidazolate framework-8 (ZIF-8) is often used for the catalytic degradation of dye wastewater, but due to its small particle size, its disadvantage of easy agglomeration prevents it from being fully functional. Herein, we report an efficient method for synthesizing biomasses/ZIF-8 using four different fruit peels as carriers. ZIF-8 nanoparticles are in-situ grown uniformly on their surface. The Brunauer–Emmett–Teller surface area of shaddock peel/ZIF-8 was found to be 752.15 m^2g^{-1}. After catalytic activity comparison, the loose shaddock peel/ZIF-8 showed the fastest and most significant degradation efficiency of 94% in methylene blue aqueous solution and could be used multiple times through a simple washing process.

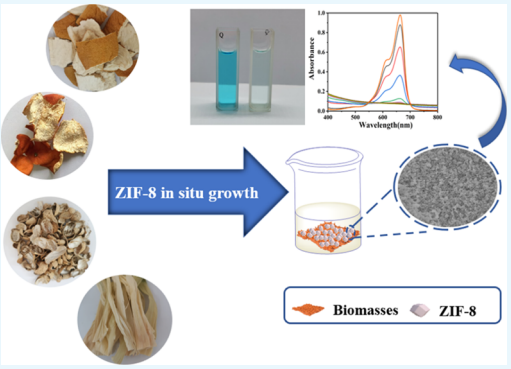

1. INTRODUCTION

The efficient use of biomass resources has great potential applicability for the urgency in decreasing environmental pollution, with the development of sustainable chemical engineering and green chemistry. Thus, the utilization of low-cost, widely sourced biomass is attractive.[1] On this basis, the easiest and most accessible biomass is plant biomass.[2] These biomasses can come from many sources, such as fruit peels, dried fruit shells, leaves, roots and seafood shells. In particular, in countries with large agricultural production, most of the waste biomasses are not used, only treated by incineration, and a large proportion is also discarded.[3−5] This universal treatment methods not only causes serious environmental pollution but also waste resources. Therefore, the use of waste biomass to produce value-added products makes our production process more environmentally friendly and can save resources.[6,7] Common ways of producing value-added products include extracting pectin, essential oils, and polysaccharides from biomass such as fruit peels with simple methods;[8,9] modifying biomass to adsorb wastewater;[10,11] and carbonizing/nitrogen-doped biomass; then, it can be used as adsorbents or conductive materials.[12−15] In addition to the method of modifying biomass, it can also be combined with other functional materials, which is also a promising way to improve performance and develop new materials.[12,16,17]

Methylene blue (MB) dye is widely used in textile, hair dyeing, printing, and other industries, resulting in a large number of MB residues in various ecosystems, causing harm to the human body and other organisms.[18] Biomass itself contains a large number of chemically active groups (carboxyl group and hydroxyl group), and its sources are wide and of low cost and can effectively remove dye molecules.[19] Therefore, with increasing environmental concern and awareness, there is a need for cost-effective technologies to remove dyes from local and industrial wastewater. Up to now, biomass materials with large porous structures and high surface area have been widely used in wastewater treatment. In particular, types of biomass or its modifications are employed for wastewater treatment.[20−23]

Metal–organic frameworks (MOFs) have provided opportunities for the development of various research fields due to their porosity, high specific surface area, and versatility, including gas storage,[24] catalysis,[25] enzyme immobilization,[26] and drug delivery.[27] The combination of MOFs with other functional materials is also a promising way to improve their performance and applicability. Many innovative materials use different materials as substrates on which MOFs grow to obtain different MOF composite membranes materials, showing a positive value in the adsorption and catalysis of dye wastewater. Among many MOF materials, zeolitic imidazolate framework (ZIF) structure materials have outstanding stability and can play their role in aqueous media.[28] Nath et al. investigate the CdSNPs@ZIF-8 prepared by encapsulating CdSNPs by the in situ method, and CdSNPs@ZIF-8 is used as a water treatment agent to degrade MB solution.[29] Park et al. used an in situ growth method to

Received: January 26, 2021
Accepted: March 26, 2021
Published: April 7, 2021

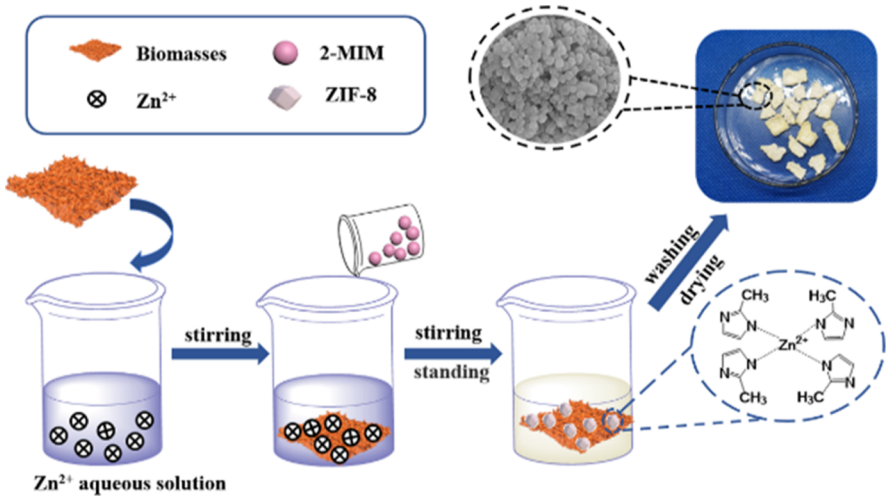

Figure 1. Schematic diagram of the biomasses/ZIF-8 preparation process by the step-by-step method.

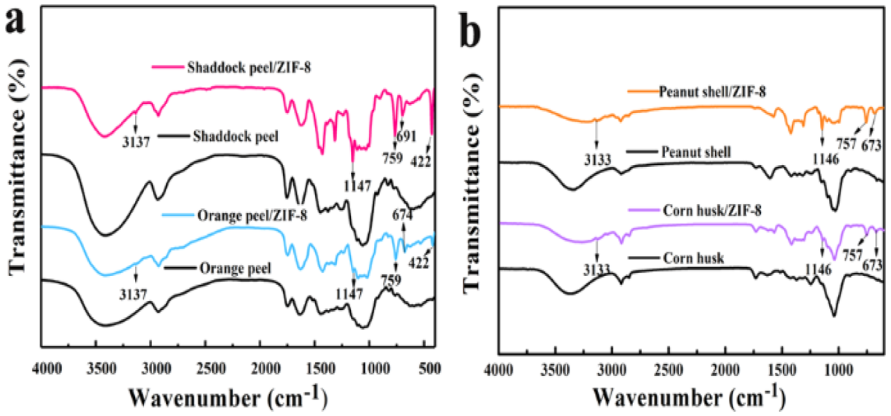

Figure 2. Infrared spectra of (a) (shaddock peel, shaddock peel/ZIF-8, orange peel, and orange peel/ZIF-8) and (b) (peanut shell, peanut shell/ZIF-8, corn husk, and corn husk/ZIF-8).

grow ZIF-8 uniformly on the surface of the filter paper and obtained a CMFP/ZIF-8 composite, which can effectively capture negatively charged organic dyes.[30] However, to the best of our knowledge, no study has reported the MOF/biomass composite catalyst fabricated from natural fruit peels. Thus, the related formation principle and its property evaluation should be investigated.

In this work, we used a step-by-step method to couple ZIF-8 to the surface of fruit peels to generate fruit peels/ZIF-8 materials and studied its ability to degrade dye wastewater and its recovery capabilities in practical applications. Many hydroxyl and carboxyl groups contained in peels provide active sites for ZIF-8 for in situ growth on the surface of fruit peels. The different numbers of functional groups in different fruit peels resulted in the difference in the content of ZIF-8. Therefore, a catalytic activity comparison was made in the degradation of MB solution. The effects of type peels, morphology, structures, and stability were also investigated. Therefore, the present work will provide a novel strategy for degrading dye wastewater and waste biomass development.

2. RESULTS AND DISCUSSION

2.1. Preparation of Biomasses/ZIF-8. As shown in Figure 1, the biomasses were first fully immersed in the zinc ion solution so that the groups on the surface interact with the zinc ions to provide a large amount of metal precursor for the production of ZIF-8, which ensures that the growth of ZIF-8 is dense on the surface of the biomasses. After adding Hmim, dense and uniform biomasses/ZIF-8 composite materials were prepared. We take orange peel/ZIF-8 as an example for illustration. Figure 1 shows the composite obtained by the in situ growth of ZIF-8 on the surface of the orange peel. This method not only reduces the agglomeration of ZIF-8 in printing and dyeing wastewater treatment, simplifying the recovery process of ZIF-8, but also makes the biomasses/ZIF-8 after simple treatment become a desirable catalyst, which can be repeatedly used to degrade MB aqueous solution.

2.2. IR Spectra. The infrared (IR) of biomass peel/ZIF-8 is shown in Figure 2. Their Fourier transform infrared spectroscopy (FT-IR) (Figure 2a) and attenuated total reflection infrared spectroscopy (ATR-IR) (Figure 2b) spectra are basically similar, indicating that these biomass surfaces have semblable functional groups. By comparing the changes before and after the growth of ZIF-8 on the biomass surface, the existence of ZIF-8 can be confirmed. It can be seen from Figure 2 that there are many absorption peaks in the infrared spectrum of pure biomasses (black lines), indicating that the surface groups from the pure biomass peels are rich and with a complex structure. The wide resonance absorption bands at 3406, 3411, 3339, and 3363 cm^{-1} are the result of O−H tensile vibration of hydroxyl and carboxyl groups in cellulose,

https://doi.org/10.1021/acsomega.1c00466
ACS Omega 2021, 6, 10187−10195

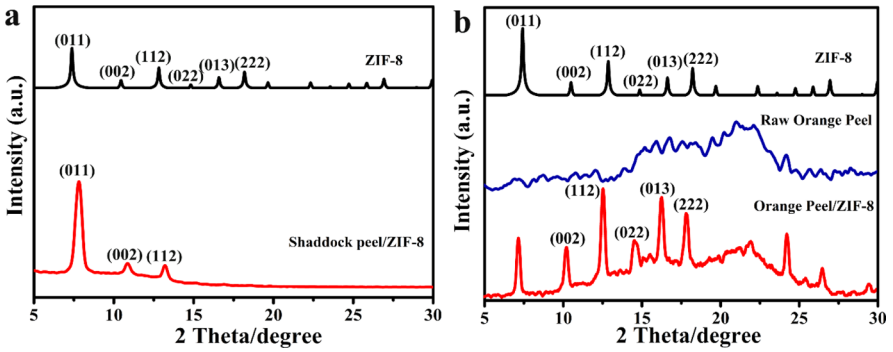

Figure 3. XRD patterns of (a) ZIF-8 and shaddock peel/ZIF-8 and (b) ZIF-8, raw orange peel, and orange peel/ZIF-8.

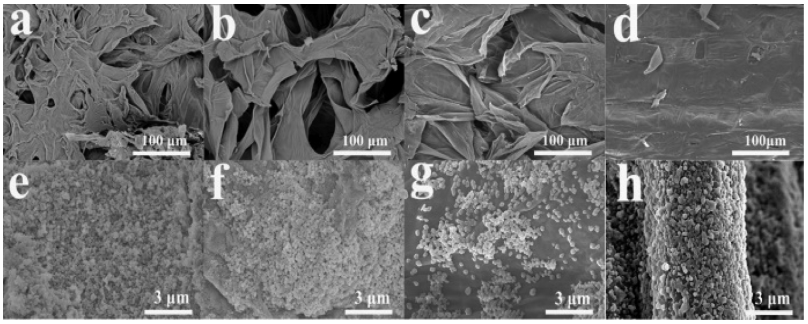

Figure 4. SEM images of ZIF-8 grown on the surface of four raw biomasses. (a) orange peel, (b) shaddock peel, (c) peanut shell, and (d) corn husk. ZIF-8 was grown on the surface of four different biomasses (e–h).

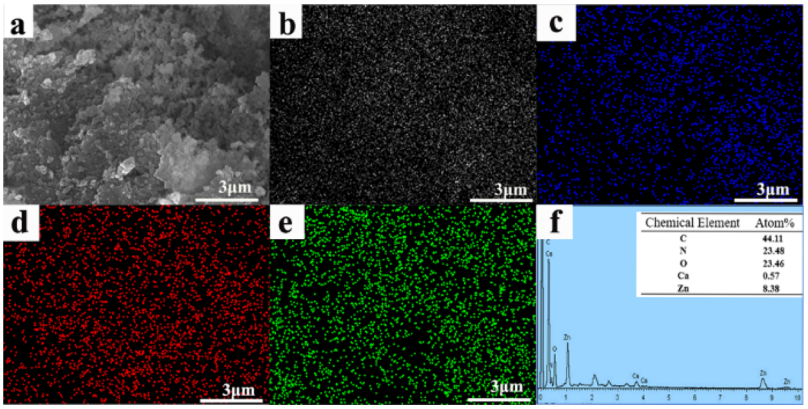

Figure 5. SEM images of orange peel/ZIF-8 (a) with the corresponding elemental mapping (b–e) of C, N, O, and Zn, respectively, and the EDS analysis (f).

indicating the existence of a large number of internal hydrogen bonds.[31−33] In addition, the reduction of the strength of cellulose O−H stretching vibration of biomasses/ZIF-8 at 3400−3200 cm^{-1} is due to the interaction between the hydroxyl group and Zn^{2+}.[34,35] The spectrum bands at 1747,1745,1735, and 1733 cm^{-1} are caused by C═O stretching vibration of the carboxyl group.[32] As shown in Figure 2a, in shaddock peel/ZIF-8 and orange peel/ZIF-8, the stretching vibration band of Zn−N is around 422 cm^{-1}. In addition, the fingerprint areas in 687 and 754 cm^{-1} spectral bands are due to Hmim ring plane bending vibration,[36] and the peak at 1146 cm^{-1} can be classified as the bending vibration of C−H on the imidazole ring and that at 1422 cm^{-1} is the stretching vibration of C−N.[37] The aliphatic and aromatic C−H stretching bands of Hmim are at around 2929 and 3137 cm^{-1}, respectively.[38] These bands indicate that ZIF-8 successfully grew on the surface of the biomasses. Due to the limitations of corn husk and peanut shell, the ATR-IR method was used for measurement in the range of 600−4000 cm^{-1}, there was no absorption peak of 422 cm^{-1}, and the vibration of stretching C═N was clearly observed to be 1574 cm^{-1}.[39,40] Moreover, other bands were similar to those in shaddock peel/ZIF-8 and orange peel/ZIF-8, and the successful growth of ZIF-8 on the surface of corn husk and peanut shell was also proved in combination with other characterizations.

2.3. X-ray Diffraction Analysis. The crystalline structure of the ZIF-8 crystals grown on different biomass peels are characterized by X-ray diffraction (XRD). Figure 3 shows the diffraction peaks of shaddock peel/ZIF-8 and orange peel/ZIF-8 at 2θ = 7.42, 10.52, 12.9, 14.83, 16.52, and 18.19°, corresponding to the (011), (002), (112), (022), (013), and (222) crystal faces of ZIF-8, respectively. It is consistent with the XRD characteristic diffraction peak position of the ZIF-8

https://doi.org/10.1021/acsomega.1c00466
ACS Omega 2021, 6, 10187−10195

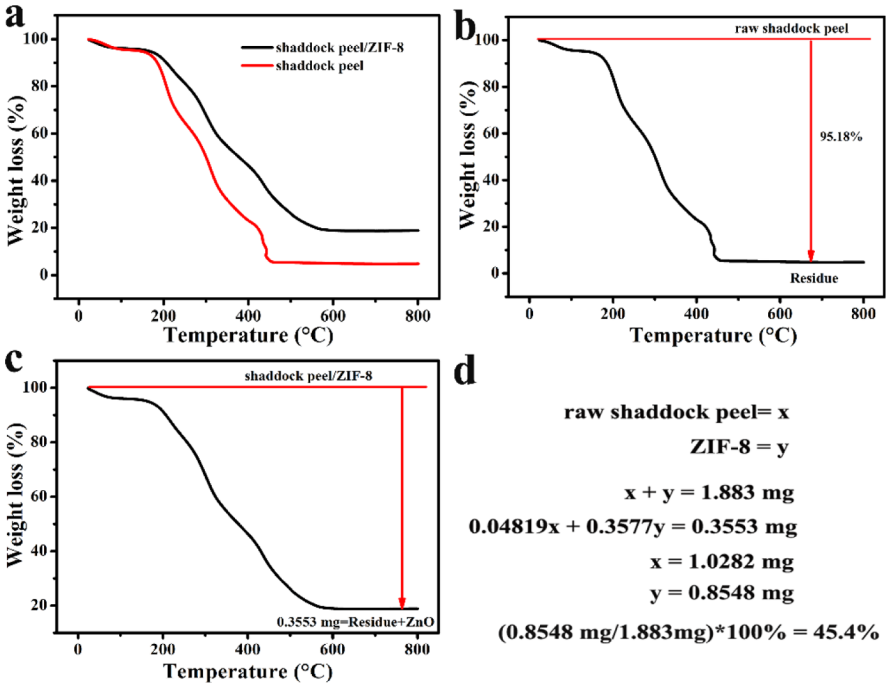

Figure 6. TGA curves of (a) shaddock peel and shaddock peel/ZIF-8, (b) raw shaddock peel, and (c) shaddock peel/ZIF-8; (d) relative amounts of ZIF-8 nanoparticles present on the shaddock peel surface were calculated from the TGA curves of shaddock peel/ZIF-8.

crystal in the literature, indicating that the obtained ZIF-8 crystal has high crystallinity.[41,42] The additional broad diffraction peaks around 2θ =16 and 21° in the XRD patterns of orange peel/ZIF-8 is associated with orange peel (Figure 3b). Similarly, the XRD of peanut shell/ZIF-8 and corn husk/ZIF-8 is shown in Figure S1, and the characteristic peaks of its ZIF-8 perfectly coincide with the characteristic peaks of simulated ZIF-8 crystals, which again demonstrates the successful synthesis of biomasses/ZIF-8.

2.4. Material Morphology. In Figure 4, the morphologies of pure biomasses and ZIF-8 growing on biomasses in situ were observed by scanning electron microscopy (SEM). Images a, b, c, and d are the scanning images of orange peel, shaddock peel, peanut shell, and corn husk, respectively. From these pictures, we can observe that there are many porous structures in orange peel and shaddock peel, which provide a large number of active sites for metal ions. The porous structure on the surface of a peanut shell is relatively sparse, with more folds, which can also increase its specific surface area. The surface of the corn husk is relatively smooth, with almost no holes and only some grooves (Figure 4g,h). As expected, due to the high porosity of orange and shaddock peels (Figure 4e,f), which provide more active sites for the growth of ZIF-8, the surface content of ZIF-8 is higher than that of peanut shells and corn husks.

2.5. EDS Mapping Image. To further confirm the component of biomasses/ZIF-8 composites, the elemental analysis of biomasses/ZIF-8 composites can be analyzed with an energy dispersive spectrometer. Figure 5 shows the distribution of elements in the orange peel/ZIF-8 composite. Since orange peel contains many natural active compounds, such as cellulose, phenolic compounds, and flavonoids,[43] they have many oxygen-containing groups. Accordingly, oxygen elements are widely distributed in Figure 5d. In addition to carbon and oxygen atoms, the uniform coverage of nitrogen and zinc atoms was also detected, indicating that the surface of orange peel was uniformly covered with ZIF-8 nanoparticles. The energy-dispersive spectroscopy (EDS)-mapping diagrams of other biomasses/ZIF-8 are shown in Figures S2 and S3. It can be concluded that the content of zinc atoms in shaddock peel/ZIF-8 and orange peel/ZIF-8 is more than that in peanut shell/ZIF-8 and corn husk/ZIF-8 composites, indicating that they contain more ZIF-8, which is consistent with Figure 4.

2.6. Thermogravimetric Analysis. In order to determine the material's thermal stability and the content of ZIF-8 in peel composites, the thermogravimetric curves of shaddock peel/ZIF-8 and shaddock peel were determined and are shown in Figure 6. As the temperature increased from room temperature to 173 °C, the mass of shaddock peel/ZIF-8 decreased slightly. At this time, the solvent molecule methanol and water in the sample will be separated from the pores or surface of ZIF-8, resulting in a slight drop in its mass. In the second stage, 35.1% of the weight occurred between 173 and 326 °C, which was attributed to the pyrolysis of cellulose shaddock peel and the volatilization of excess Hmim, since the ligand Hmim has a boiling point of 267 °C. In the third stage, a 40.63% weight loss occurred between 326 and 750 °C due to the oxidation of ZIF-8 to ZnO and pyrolysis of lignin of shaddock peel. The amounts of ZIF-8 present on shaddock peel were calculated from the thermogravimetric analysis (TGA) curves (Figure 6d). The calculated result indicates that the content of ZIF-8 in shaddock peel/ZIF-8 is 45.4%.

2.7. Porosity Properties. Furthermore, the porosity properties are usually evaluated by N_2 adsorption−desorption isotherms. Figure S4 shows the corresponding adsorption and desorption isotherm of biomasses/ZIF-8 composites which is derived from the Brunauer−Emmett−Teller (BET) theory, in which the insets are the pore size distribution calculated by HK and BJH methods. The adsorption results in Figure S4 showed that the four biomasses/ZIF-8 exhibit type I isotherm, which are characteristic features of the MOF's microporous structure. The adsorption volume increases rapidly at low pressure (P/P_0

https://doi.org/10.1021/acsomega.1c00466
ACS Omega 2021, 6, 10187−10195

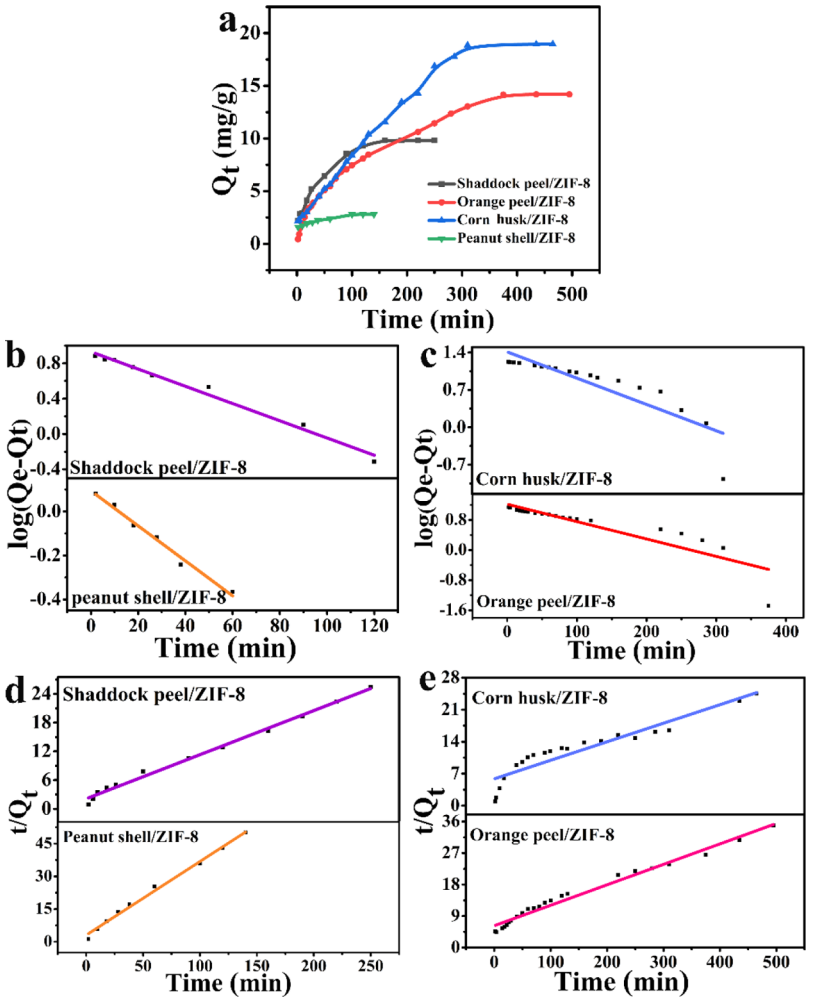

Figure 7. (a) Kinetics of adsorption of MB by different biomasses/ZIF-8; (b,c) pseudo-first-order kinetic mode of four biomasses/ZIF-8; and (d,e) pseudo-second-order kinetic model of four biomasses/ZIF-8.

is less than 0.1), which is the result of the micropore filling of shaddock peel/ZIF-8. According to the micropore distribution method, the pore size of shaddock peel/ZIF-8 is concentrated at 0.65 nm. The second increase in the adsorption volume when the relative pressure is 0.9−1.0 indicates that there are meso/macropores in the shaddock peel/ZIF-8 structure, which is consistent with the SEM result (Figure 4b). The BET specific surface area, Langmuir specific surface area, and total single-point adsorption volume of shaddock peel/ZIF-8 are 752.15 m^2g^{-1}, 770.39 m^2g^{-1}, and 0.52 cm^3g^{-1}, respectively. Compared with shaddock peel/ZIF-8, orange peel/ZIF-8, peanut shell/ZIF-8, and corn husk/ZIF-8 all had lower BET specific surface area (40.16, 27.66, and 28.31 m^2g^{-1}, respectively), which was caused by the abundant porous structure of shaddock peel and more active groups on the surface than other biomass surfaces.

2.8. Adsorption Kinetics of MB to Biomasses/ZIF-8. The difference in the nature and structure of the biomasses themself leads to different abilities to adsorb MB. In order to illustrate this problem, four pure biomasses were used as adsorbents, and experiments of MB adsorption were carried out. The results showed that pure corn husk adsorbed MB the most, at 5.38 mg/g, which was consistent with the results of static kinetic adsorption. The static kinetic curve of biomasses/ZIF-8 adsorption of MB is shown in Figure 7. The corn husk/ZIF-8 exhibits the strongest adsorption capacity, adsorption capacity is 18.95 mg/g, while the adsorption equilibrium time needed is relatively long, and shaddock peel/ZIF-8, orange peel/ZIF-8, and peanut shell/ZIF-8 adsorption was 9.82, 14.18, and 2.79 mg/g, independently. In addition to the role of ZIF-8, the adsorption of MB by corn husk itself leads to the strongest adsorption capacity among the four biomasses.

Table 1 shows the parameters obtained by fitting the kinetic adsorption process. The correlation coefficient of the pseudo-second-order kinetic curve is higher than that of the pseudo-first-order kinetics, indicating that the adsorption of biomasses/ZIF-8 to MB is more in line with the pseudo-second-order kinetic model, where the rate constant k_2 is the expected biomasses/ZIF-8 diffusion-limited behavior.

Table 1. List of the Pseudo-First-Order and the Pseudo-Second-Order Kinetic Rate and Correlation Coefficient R^2 of Biomasses/ZIF-8

	pseudo-first-order		pseudo-second-order	
samples	K_1 (min^{-1})	R^2	K_2 (min^{-1})	R^2
shaddock peel/ZIF-8	0.0351	0.9839	0.0921	0.9933
orange peel/ZIF-8	0.00811	0.7723	0.0584	0.9795
peanut shell/ZIF-8	0.0958	0.9826	0.0328	0.9926
corn bran/ZIF-8	0.00682	0.7590	0.0406	0.8633

https://doi.org/10.1021/acsomega.1c00466
ACS Omega 2021, 6, 10187−10195

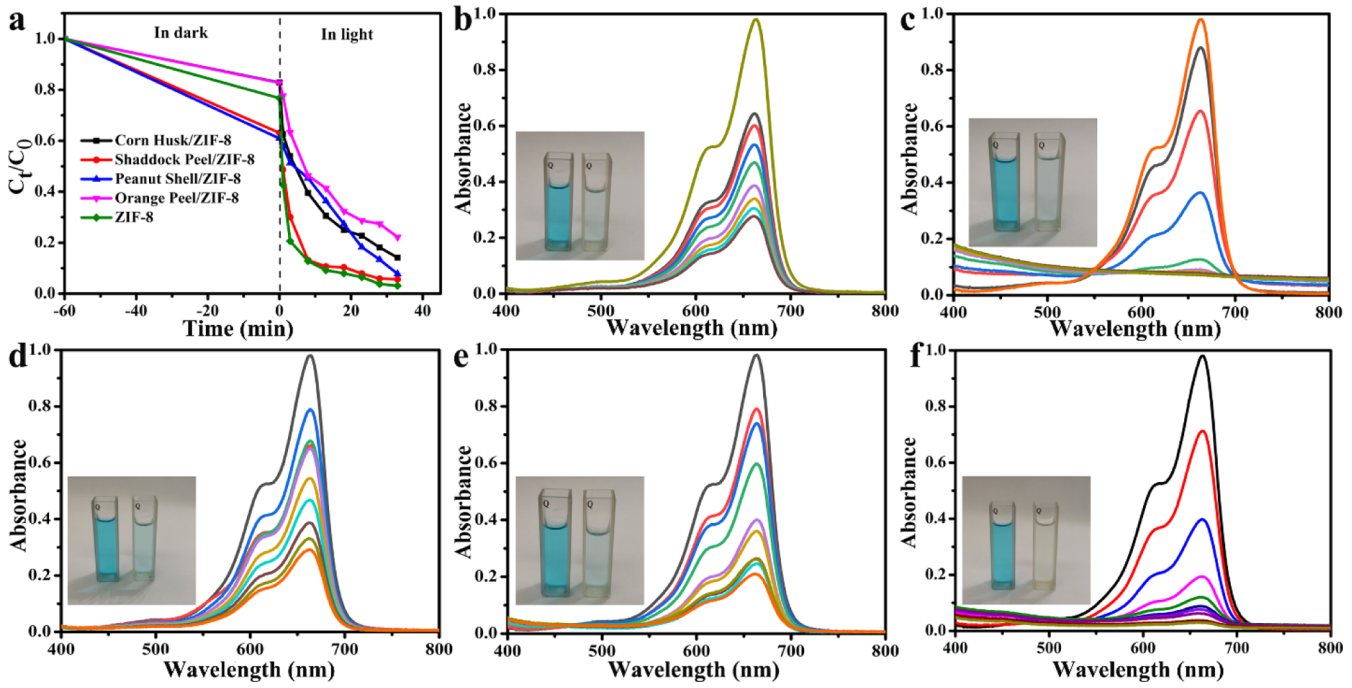

Figure 8. (a) Photocatalytic performance of all catalysts, (b–f) UV–visible absorption spectrum of MB dye solution catalyzed by corn husk/ZIF-8, shaddock peel/ZIF-8, peanut shell/ZIF-8, orange peel/ZIF-8, and ZIF-8, respectively.

2.9. Photodegradation of MB. It is well known that ZIF-8 has been widely used in catalysis. In order to further verify the success of in situ growth of ZIF-8 on the biomass surface, its certain advantages in performance were determined. Before the degradation experiment, the biomasses/ZIF-8 composites were cut into small strips or chopped, which was more conducive to the degradation of dyes. MB is widely used in the dye industry, so it is chosen as the model dye for this degradation experiment. MB was degraded to other substances under light conditions and changed in the spectrum.

The photocatalytic performance of different biomasses/ZIF-8 and ZIF-8 on MB was evaluated (Figure 8a). There is no doubt that ZIF-8 has the highest photodegradation efficiency under the same conditions, which can reach 96.9%. The degradation efficiencies of shaddock peel/ZIF-8, corn husk/ZIF-8, peanut shell/ZIF-8, and orange peel/ZIF-8 were 94, 85.9, 92, and 79%, respectively. The low degradation efficiency of biomasses/ZIF-8 is because it includes the weight of biomass itself, resulting in a relatively small amount of ZIF-8 actually used in the catalytic process. It is gratifying that the degradation efficiency of shaddock peel/ZIF-8 is not much different from that of ZIF-8, and it has the advantage of being easily separated from the solution and reused. The photocatalytic stability of the shaddock peel/ZIF-8 composite was studied by the photocatalytic reaction of MB several times. As can be seen from Figure S5, after three cycles of degradation of MB by the shaddock peel/ZIF-8 composite material, the photocatalytic activity did not significantly decline, and the degradation efficiency could still reach 76%, indicating that the catalyst shaddock peel/ZIF-8 in this study has excellent photostability under illumination. It can be seen from Figure 8b–f that the MB solution is degraded by different catalysts, and its absorbance also changes accordingly. In addition, the degradation performance of shaddock peel/ZIF-8 and pectin/ZIF-8 was compared to evaluate the peeling performance of ZIF-8. It can be seen from Figure S6 that there is no significant difference in degradation of MB dye between shaddock peel/ZIF-8 and pectin/ZIF-8. However, the removal effect of pectin/ZIF-8 on dyes depends more on adsorption, which may be related to the properties of pectin itself. The amount of ZIF-8 on the pectin surface is small, and its reusability is poor due to its shedding.

To better assess the ability of degradation of shaddock peel/ZIF-8, we have compared our results with relevant reports using ZIF-8 composite-based nanomaterials as photocatalysts. Compared with other work,[44,45] under the condition of a similar degradation rate, the degradation time of MB by shaddock peel/ZIF-8 is greatly reduced. Because the preparation method of shaddock peel/ZIF-8 is simple, the raw materials are cheap and easy to obtain, and it shows that shaddock peel/ZIF-8 has a good prospect for dye photodegradation.

3. CONCLUSIONS

In summary, we used common shaddock peel, orange peel, corn husk, and peanut shell as the base material to prepare biomasses/ZIF-8, which solved the problem of small particle size and easy agglomeration of ZIF-8 and expanded the scope of application of biomasses. Because of the difference in the active groups and specific surface area of different biomasses, biomasses/ZIF-8 exhibits diversity in the degradation of MB solution. The degradation efficiency of four different biomasses/ZIF-8 to MB solution was compared, and the degradation efficiency of shaddock peel/ZIF-8, orange peel/ZIF-8, corn husk/ZIF-8, and peanut shell/ZIF-8 is 94, 79, 92, and 85.9%, respectively. Shaddock peel has the advantages of a rich porous structure and larger specific surface area, so the degradation efficiency is the highest among the four composites. Moreover, the degradation efficiency of shaddock peel/ZIF-8 and pectin/ZIF-8 on MB was also compared, and it was found that the degradation efficiency of MB solution was still up to 76% after three cycles of shaddock peel/ZIF-8.

https://doi.org/10.1021/acsomega.1c00466
ACS Omega 2021, 6, 10187−10195

Consequently, shaddock peel/ZIF-8 may be an admirable catalyst with high selectivity. Due to the wide variety of biomasses and each having its unique spatial structure and chemical characteristics, the selective adsorption and catalytic degradation of organic dyes are expected.

Moreover, various MOFs/biomass porous composites can be obtained using the reported method when assisted by different ligands, metal ions, and peels containing carbohydrates. These porous composites could be applied to wastewater treatment and adsorption separation fields, in which hierarchical porous structures could efficiently resolve mass transfer resistance. We will devote ourselves to looking for some new ways to form chemical bond linkages between MOFs and other biomasses, as well as develop their application in our future work.

4. MATERIALS AND METHODS

4.1. Materials. Fresh ripe orange peel (*Citrus sinensis*), shaddock peel, corn husk, and peanut shell were purchased from the local fruit vendors in Xinjiang (China). $(Zn(NO_3)_2)\cdot 6H_2O$ and methanol were obtained from Tianjin ZhiYuan company, 2-methylimidazole (Hmim) and MB were purchased from Aladdin Co. (China), and pectin was obtained from YuHua biotechnology company. Deionized water was used in all related experiments of this work. Besides biomasses, all reagents were used as received without any further purification.

4.2. Preparation of Orange Peel/ZIF-8. Washed orange peel, shaddock peel, corn husk, and peanut shell were cut into small pieces approximately 1 × 1 cm and then dried in the oven for 2 h. $(Zn(NO_3)_2)\cdot 6H_2O$ (0.975 g) was dissolved in a mixed solution of 25 mL of methanol and 25 mL of water, and 0.45 g of the treated fruit peels was added in the zinc ion solution and stirred for 8 h. Subsequently, 2.45 g of Hmim was dissolved in a mixture of methanol and water in the same proportion. After it was completely dissolved, it was then mixed with zinc ion solutions, stirred for 8 h, and then allowed to stand at room temperature for 24 h. Next, the biomasses/ZIF-8 was washed with methanol three times to remove any unreacted precursors. Finally, it was dried for 4 h under vacuum at 60 °C. The preparation steps of ZIF-8 are the same.

4.3. Preparation of Pectin/ZIF-8. Pectin (0.8 g) was added to 10 mL of distilled water and stirred until it completely dissolved. Then, an appropriate amount of glutaraldehyde was added and stirred for 2 h to cross-link. They were then spread evenly over the surface of the Petri dish and dried naturally at room temperature. Then, 0.45 g of the pectin film was immersed in a solution of zinc ions containing the same amount of water and methanol, stirred for 8 h, added Hmim, and continued stirring for 8 h. After standing for 24 h, it was washed with methanol three times and dried.

4.4. Characterization. The morphologies of different biomass peel/ZIF-8 were observed using a Hitachi S-4800 scanning electron microscope equipped with an EDS detector. The FT-IR and ATR-IR of the biomasses/ZIF-8 were also measured in the range of 400−4000 cm^{-1} wavenumber through the Bruker Vertex 70 table. The biomasses/ZIF-8 was processed first; then, the impurities were removed, and then, the XRD test was performed on a Bruker D8 Advance ($\lambda K\alpha$ = 1.5418 Å, 2θ = 10−80°). The porosity properties of biomasses peel/ZIF-8 were characterized by N_2 adsorption−desorption isotherms on a Kubo-X1000. TGA (Netzsch STA-449c) was used to study the thermal stability of materials heated at a rate of 10 °C/min from room temperature to 1000 °C under nitrogen.

4.5. Adsorption Experiment. To investigate the adsorption capacities, the biomasses/ZIF-8 was cut into pieces, and about 30 mg of the pieces was put into a glass bottle containing 100 mL of MB solution with an initial concentration of 20 mg/L. In addition, the adsorption experiment carried out static adsorption under dark conditions until the equilibrium time was reached. To study the static adsorption properties, the concentration of MB solution at the same time intervals was measured using a UV-2550 spectrophotometer (Shimadzu Co., Ltd., Japan) at a wavelength of 664 nm. The adsorption capacity (Q_e) of the biomasses/ZIF-8 adsorbents was calculated using the following equation

$$Q_e = \frac{(C_0 - C_e)}{m} V \tag{1}$$

where C_0 is the initial MB concentration, C_e is the concentration of MB at adsorption equilibrium, V is the volume of solution, and m is the mass of the biomasses/ZIF-8 composites.

The adsorption process of biomasses/ZIF-8 over time was analyzed using quasi-first-order and quasi-second-order kinetic models, which were as follows

$$\log(Q_e - Q_t) = \log Q_e - \frac{k_1 t}{2.303} \tag{2}$$

$$\frac{t}{Q_t} = \frac{1}{k_2 Q_e^{\,2}} + \frac{t}{Q_e} \tag{3}$$

Where Q_e and Q_t are the adsorption capacity at equilibrium and at time t and k_1 and k_2 are the rate constants of the quasi-first-order model and quasi-second-order model, respectively.

4.6. Photodegradation of MB. The photodegradation experiment was performed at room temperature. Biomasses/ZIF-8 was ground into powder or cut into very thin strips; then, 20 mg of different biomasses/ZIF-8 was added into 50 mL of MB aqueous solution (10 mg/L). The adsorption was carried out under dark conditions. After the adsorption reached saturation, the solution was placed under a 300 w xenon lamp under simulated sunlight conditions for photocatalytic degradation, and the irradiation distance of the mixed solution and the lamp was about 15 cm. In a certain time interval, 3 mL of the solution was taken to measure the concentration change using a UV−vis spectrometer, and the maximum absorption wavelength of MB is 664 nm.

■ ASSOCIATED CONTENT

Supporting Information

The Supporting Information is available free of charge at https://pubs.acs.org/doi/10.1021/acsomega.1c00466.

XRD patterns of ZIF-8, raw corn husk, and corn husk/ZIF-8 and ZIF-8, raw peanut shell, and peanut shell/ZIF-8; SEM image and SEM/EDS point graph of the corresponding color coding of biomasses/ZIF-8; EDS analysis of corn husk/ZIF-8, peanut shell/ZIF-8, and shaddock peel/ZIF-8; N_2 adsorption−desorption isotherms of biomasses/ZIF-8; recyclable experiments of the shaddock peel/ZIF-8 catalyst for the degradation of MB, under visible light irradiation for three repeated cycles; photocatalytic degradation of MB solution by

https://doi.org/10.1021/acsomega.1c00466
ACS Omega 2021, 6, 10187−10195

pectin/ZIF-8 and shaddock peel/ZIF-8 and photograph of comparison of degraded MB solution of pectin/ZIF-8 (left) and shaddock peel/ZIF-8 (right); and comparison of the degradation ability of MB solution (PDF)

AUTHOR INFORMATION

Corresponding Author

Liqin Cao − *Key Laboratory of Oil and Gas Fine Chemicals, Ministry of Education & Xinjiang Uygur Autonomous Region, Xinjiang University, Urumqi 830046, P. R. China;* orcid.org/0000-0003-1551-5982; Email: cao_lq@163.com

Authors

Lu Liu − *Key Laboratory of Oil and Gas Fine Chemicals, Ministry of Education & Xinjiang Uygur Autonomous Region, Xinjiang University, Urumqi 830046, P. R. China*

Hongyan Niu − *Key Laboratory of Oil and Gas Fine Chemicals, Ministry of Education & Xinjiang Uygur Autonomous Region, Xinjiang University, Urumqi 830046, P. R. China*

Jide Wang − *Key Laboratory of Oil and Gas Fine Chemicals, Ministry of Education & Xinjiang Uygur Autonomous Region, Xinjiang University, Urumqi 830046, P. R. China*

Complete contact information is available at: https://pubs.acs.org/10.1021/acsomega.1c00466

Notes

The authors declare no competing financial interest.

ACKNOWLEDGMENTS

The authors acknowledge the research grant provided by the National Natural Science Foundation of China (no. 51763020 and no. 51963019). The authors also thank the test platform in the Ministry Key Laboratory of Oil and Gas Fine Chemicals for assistance with the UV−visible spectroscopic measurements.

REFERENCES

(1) Lei, L.; Wang, Y.; Zhang, Z.; An, J.; Wang, F. Transformations of biomass, its derivatives and downstream chemicals over ceria catalysts. *ACS Catal.* **2020**, *10*, 8788−8814.

(2) Mani, D.; Kumar, C. Biotechnological advances in bioremediation of heavy metals contaminated ecosystems: an overview with special reference to phytoremediation. *Int. J. Environ. Sci. Technol.* **2014**, *11*, 843−872.

(3) Huang, X.; Li, M.; Li, J.; Song, Y. A high-resolution emission inventory of crop burning in fields in China based on MODIS Thermal Anomalies/Fire products. *Atmos. Environ.* **2012**, *50*, 9−15.

(4) Ding, A. J.; Fu, C. B.; Yang, X. Q.; Sun, J. N.; Petäjä, T.; Kerminen, V.-M.; Wang, T.; Xie, Y.; Herrmann, E.; Zheng, L. F.; Nie, W.; Liu, Q.; Wei, X. L.; Kulmala, M. Intense atmospheric pollution modifies weather: a case of mixed biomass burning with fossil fuel combustion pollution in eastern China. *Atmos. Chem. Phys.* **2013**, *13*, 10545−10554.

(5) Singh, D. P.; Gadi, R.; Mandal, T. K.; Saud, T.; Saxena, M.; Sharma, S. K. Emissions estimates of PAH from biomass fuels used in rural sector of Indo-Gangetic Plains of India. *Atmos. Environ.* **2013**, *68*, 120−126.

(6) Güzel, N.; Kahraman, O.; Feng, H. Solid−liquid extraction by manothermosonication: recapturing the value of pomegranate peels and nano complexation of extracts with pea protein. *ACS Sustainable Chem. Eng.* **2020**, *8*, 16671−16679.

(7) Yin, H.; Lu, B.; Xu, Y.; Tang, D.; Mao, X.; Xiao, W.; Wang, D.; Alshawabkeh, A. N. Harvesting capacitive carbon by carbonization of waste biomass in molten salts. *Environ. Sci. Technol.* **2014**, *48*, 8101−8108.

(8) Gómez, B.; Gullón, B.; Remoroza, C.; Schols, H. A.; Parajó, J. C.; Alonso, J. L. Purification, characterization, and prebiotic properties of pectic oligosaccharides from orange peel wastes. *J. Agric. Food Chem.* **2014**, *62*, 9769−9782.

(9) Ciriminna, R.; Fidalgo, A.; Avellone, G.; Carnaroglio, D.; Danzì, C.; Timpanaro, G.; Meneguzzo, F.; Ilharco, L. M.; Pagliaro, M. Economic and technical feasibility of betanin and pectin extraction from opuntia ficus-indica peel via Microwave-Assisted hydrodiffusion. *ACS Omega* **2019**, *4*, 12121−12124.

(10) Herrera, A.; Tejada-Tovar, C.; González-Delgado, Á. D. Enhancement of cadmium adsorption capacities of agricultural residues and industrial fruit byproducts by the incorporation of Al_2O_3 nanoparticles. *ACS Omega* **2020**, *5*, 23645−23653.

(11) Zhu, G.; Xing, X.; Wang, J.; Zhang, X. Effect of acid and hydrothermal treatments on the dye adsorption properties of biomass-derived activated carbon. *J. Mater. Sci.* **2017**, *52*, 7664−7676.

(12) Zhao, Y.; Shi, J.; Wang, X.; Li, W.; Wu, Y.; Jiang, Z. Biomass@MOF-derived carbon aerogels with a hierarchically structured surface for treating organic pollutants. *Ind. Eng. Chem. Res.* **2020**, *59*, 17529−17536.

(13) Dan, R.; Chen, W.; Xiao, Z.; Li, P.; Liu, M.; Chen, Z.; Yu, F. N-Doped biomass carbon/reduced graphene oxide as a high-performance anode for sodium-ion batteries. *Energy Fuels* **2020**, *34*, 3923−3930.

(14) Tian, M.; Zhu, Y.; Zhang, D.; Wang, M.; Chen, Y.; Yang, Y.; Gao, S. Pyrrolic-nitrogen-rich biomass-derived catalyst for sustainable degradation of organic pollutant via a self-powered electro-fenton process. *Nano Energy* **2019**, *64*, 103940.

(15) Wang, J.; Ma, C.; Su, L.; Gong, L.; Dong, D.; Wu, Z. Self-assembly/sacrificial synthesis of highly capacitive hierarchical porous carbon from longan pulp biomass. *ChemElectroChem* **2020**, *7*, 4606−4613.

(16) Salgaonkar, M.; Nadar, S. S.; Rathod, V. K. Biomineralization of orange peel peroxidase within metal organic frameworks (OPP−MOFs) for dye degradation. *J. Environ. Chem. Eng.* **2019**, *7*, 102969.

(17) Xie, T.; Wang, J.; Liu, X.; Shang, Y.; Ma, C.; Su, L.; Gong, L. Hierarchical porous activated carbon derived from enteromorpha prolifera for superior electrochemical capacitive behavior. *Ionics* **2020**, *26*, 403−413.

(18) Ghaedi, M.; Heidarpour, S.; Nasiri Kokhdan, S.; Sahraie, R.; Daneshfar, A.; Brazesh, B. Comparison of silver and palladium nanoparticles loaded on activated carbon for efficient removal of methylene blue: kinetic and isotherm study of removal process. *Powder Technol.* **2012**, *228*, 18−25.

(19) Mohan, D.; Sarswat, A.; Ok, Y. S.; Pittman, C. U., Jr. Organic and inorganic contaminants removal from water with biochar, a renewable, low cost and sustainable adsorbent—a critical review. *Bioresour. Technol.* **2014**, *160*, 191−202.

(20) Pang, N.; Bergeron, A. D.; Gu, X.; Fu, X.; Dong, T.; Yao, Y.; Chen, S. Recycling of nutrients from dairy wastewater by extremophilic microalgae with high ammonia tolerance. *Environ. Sci. Technol.* **2020**, *54*, 15366−15375.

(21) Guo, Z.; Zhang, X.; Kang, Y.; Zhang, J. Biomass-derived carbon sorbents for Cd (II) removal: Activation and adsorption mechanism. *ACS Sustainable Chem. Eng.* **2017**, *5*, 4103−4109.

(22) Roy, A.; Chakraborty, S.; Kundu, S. P.; Adhikari, B.; Majumder, S. B. Adsorption of anionic-azo dye from aqueous solution by lignocellulose-biomass jute fiber: Equilibrium, kinetics, and thermodynamics study. *Ind. Eng. Chem. Res.* **2012**, *51*, 12095−12106.

(23) Herrera, A.; Tejada-Tovar, C.; González-Delgado, Á. D. Enhancement of cadmium adsorption capacities of agricultural residues and industrial fruit byproducts by the incorporation of Al_2O_3 nanoparticles. *ACS Omega* **2020**, *5*, 23645−23653.

(24) Henkelis, S. E.; Judge, P. T.; Hayes, S. E.; Nenoff, T. M. Preferential SO_x adsorption in Mg-MOF-74 from a humid acid gas stream. *ACS Appl. Mater. Interfaces* **2021**, *13*, 7278−7284.

(25) Wang, C.; An, B.; Lin, W. Metal−organic frameworks in solid−gas phase catalysis. *ACS Catal.* **2018**, *9*, 130−146.
(26) Ulu, A. Metal-organic frameworks (MOFs): A novel support platform for ASNase immobilization. *J. Mater. Sci.* **2020**, *55*, 6130−6144.
(27) Abazari, R.; Mahjoub, A. R.; Ataei, F.; Morsali, A.; Carpenter-Warren, C. L.; Mehdizadeh, K.; Slawin, A. M. Z. Chitosan immobilization on Bio-MOF nanostructures: A biocompatible pH-responsive nanocarrier for doxorubicin release on MCF-7 cell lines of human breast cancer. *Inorg. Chem.* **2018**, *57*, 13364−13379.
(28) Phan, A.; Doonan, C. J.; Uribe-Romo, F. J.; Knobler, C. B.; O'Keeffe, M.; Yaghi, O. M. Synthesis, structure, and carbon dioxide capture properties of zeolitic imidazolate frameworks. *Acc. Chem. Res.* **2010**, *43*, 58−67.
(29) Malik, A.; Nath, M.; Mohiyuddin, S.; Packirisamy, G. Multifunctional CdSNPs@ZIF-8: potential antibacterialagent against GFP-Expressing Escherichia coli and staphylococcus aureus and efficient photocatalyst for degradation of methylene blue. *ACS Omega* **2018**, *3*, 8288−8308.
(30) Park, J.; Oh, M. Construction of flexible metal-organic framework (MOF) papers through MOF growth on filter paper and their selective dye capture. *Nanoscale* **2017**, *9*, 12850−12854.
(31) Aggrawal, S.; Chauhan, I.; Mohanty, P. Immobilization of Bi_2O_3 nanoparticles on the cellulose fibers of paper matrices and investigation of its antibacterial activity against E. coli in visible light. *Mater. Express* **2015**, *5*, 429−436.
(32) Thirumavalavan, M.; Lai, Y.-L.; Lee, J.-F. Fourier transform infrared spectroscopic analysis of fruit peels before and after the adsorption of heavy metal ions from aqueous solution. *J. Chem. Eng. Data* **2011**, *56*, 2249−2255.
(33) Chen, J.; Yu, Y.; Shang, Q.; Han, J.; Liu, C. Enhanced oil adsorption and nano-emulsion separation of nanofibrous aerogels by coordination of pomelo peel-derived biochar. *Ind. Eng. Chem. Res.* **2020**, *59*, 8825−8835.
(34) Chauhan, I.; Aggrawal, S.; Mohanty, P. ZnO nanowire-immobilized paper matrices for visible light-induced antibacterial activity against Escherichia coli. *Environ. Sci.: Nano* **2015**, *2*, 273−279.
(35) Chauhan, I.; Mohanty, P. Immobilization of titania nanoparticles on the surface of cellulose fibres by a facile single step hydrothermal method and study of their photocatalytic and antibacterial activities. *RSC Adv.* **2014**, *4*, 57885−57890.
(36) Jian, M.; Liu, B.; Zhang, G.; Liu, R.; Zhang, X. Adsorptive removal of arsenic from aqueous solution by zeolitic imidazolate framework-8 (ZIF-8) nanoparticles. *Colloids Surf., A* **2015**, *465*, 67−76.
(37) Yao, J.; Chen, R.; Wang, K.; Wang, H. Direct synthesis of zeolitic imidazolate framework-8/chitosan composites in chitosan hydrogels. *Microporous Mesoporous Mater.* **2013**, *165*, 200−204.
(38) Low, Z.-X.; Yao, J.; Liu, Q.; He, M.; Wang, Z.; Suresh, A. K.; Bellare, J.; Wang, H. Crystal transformation in zeolitic-imidazolate framework. *Cryst. Growth Des.* **2014**, *14*, 6589−6598.
(39) Bhattacharyya, S.; Pang, S. H.; Dutzer, M. R.; Lively, R. P.; Walton, K. S.; Sholl, D. S.; Nair, S. Interactions of SO_2-containing acid gases with ZIF-8: structural changes and mechanistic investigations. *J. Phys. Chem. C* **2016**, *120*, 27221−27229.
(40) Gadipelli, S.; Travis, W.; Zhou, W.; Guo, Z. A thermally derived and optimized structure from ZIF-8 with giant enhancement in CO2 uptake. *Energy Environ. Sci.* **2014**, *7*, 2232−2238.
(41) Zhu, M.; Venna, S. R.; Jasinski, J. B.; Carreon, M. A. Room-temperature synthesis of ZIF-8: The coexistence of ZnO nanoneedles. *Chem. Mater.* **2011**, *23*, 3590−3592.
(42) Chen, Z.; Liu, M.; Wu, R. Strongly coupling of Co_9S_8/Zn-Co-S heterostructures rooted in carbon nanocages towards efficient oxygen evolution reaction. *J. Catal.* **2018**, *361*, 322−330.
(43) Rafiq, S.; Kaul, R.; Sofi, S. A.; Bashir, N.; Nazir, F.; Ahmad Nayik, G. Citrus peel as a source of functional ingredient: A review. *J. Saudi Soc. Agric. Sci.* **2018**, *17*, 351−358.
(44) Kirchon, A.; Zhang, P.; Li, J.; Joseph, E. A.; Chen, W.; Zhou, H.-C. Effect of isomorphic metal substitution on the fenton and photo-fenton degradation of methylene blue using Fe-based metal−organic frameworks. *ACS Appl. Mater. Interfaces* **2020**, *12*, 9292−9299.
(45) Wang, Y.; Ge, S.; Cheng, W.; Hu, Z.; Shao, Q.; Wang, X.; Lin, J.; Dong, M.; Wang, J.; Guo, Z. Microwave hydrothermally synthesized metal−organic framework-5 derived C-doped ZnO with enhanced photocatalytic degradation of rhodamine B. *Langmuir* **2020**, *36*, 9658−9667.

https://doi.org/10.1021/acsomega.1c00466
ACS Omega 2021, 6, 10187−10195